



Article

Estimating Regional Soil Moisture Distribution Based on NDVI and Land Surface Temperature Time Series Data in the Upstream of the Heihe River Watershed, Northwest China

Xiao Bai ¹, Lanhui Zhang ^{1,†}, Chansheng He ^{1,2,*,†} and Yi Zhu ¹

¹ Key Laboratory of West China's Environmental System (Ministry of Education), Center for Dryland Water Resources Research and Watershed Science, College of Earth and Environmental Sciences, Lanzhou University, Lanzhou 730000, China; ibaixiao@hotmail.com (X.B.); lh Zhang@lzu.edu.cn (L.Z.); zhuy15@lzu.edu.cn (Y.Z.)

² Department of Geography, Western Michigan University, Kalamazoo, MI 49008, USA

* Correspondence: he@wmich.edu

† These authors contributed equally to this work.

Received: 10 June 2020; Accepted: 24 July 2020; Published: 28 July 2020



Abstract: Temporal and spatial variability of soil moisture has an important impact on hydrological processes in mountainous areas. Understanding such variability requires soil moisture datasets at multiple temporal and spatial scales. Remote sensing is a very effective method to obtain surface (~5 cm depth) soil moisture at the regional scale but cannot directly measure soil moisture at deep soil layers (>5 cm depth) currently. This study chose the upstream of the Heihe River Watershed in the Qilian Mountain Ranges in Northwest China as the study area to estimate the profile soil moisture (0–70 cm depth) at the regional scale using satellite Vegetation Index (NDVI) and Land Surface Temperature (LST) products. The study area was divided into 31 zones according to the combination of altitude, vegetation and soil type. Long-term in situ soil moisture observation stations were set up at each of the zones. Soil moisture probe, ECH2O, was used to collect soil moisture at five layers (0–10, 10–20, 20–30, 30–50 and 50–70 cm) continuously. Multiple linear regression equations of time series MODIS (Moderate-resolution Imaging Spectroradiometer) NDVI, LST and soil moisture were developed for each of the five soil layers at the 31 zones to estimate the soil moisture (0–70 cm) on a regional scale with a spatial resolution of 1 km² and a temporal resolution of 16-d from October, 2013 to September, 2016. The correlation coefficient R of the regression equations was between 0.47 and 0.94, the RMSE was 0.03, indicating that the estimation method based on the MODIS NDVI and LST data was suitable and could be applied to alpine mountainous areas with complex topography, soil and vegetation types. The overall pattern of soil moisture spatial distribution indicated that soil moisture was higher in the eastern region than in the western region, and the soil moisture content in the whole study area was 14.5%. The algorithm and results provide novel applications of remote sensing to support soil moisture data acquisition and hydrological research in mountainous areas.

Keywords: soil moisture estimation; in situ observations; MODIS NDVI and LST; soil moisture variability; the Heihe River watershed

1. Introduction

Soil moisture is an essential component of the terrestrial water cycle, and serves as a critical link between the precipitation, surface water, groundwater and vegetation water [1–6]. It plays an important role in hydrological processes and land surface–atmosphere interactions

such as the Soil–Plant–Atmosphere Continuum (SPAC) [7]. Mountains are water towers of rivers, and understanding the distribution of soil moisture over the mountainous areas, is essential for hydrological modeling and water resources management, especially in arid areas, such as Northwest China [8]. Since its strong temporal and spatial variability, soil moisture has an important effect on the distribution of regional water resources, and ecosystem services [9–11]. Unfortunately, the impact of soil moisture on both hydrological processes and ecosystem services over the regional scale has been poorly understood due to the lack of long-term, large-scale soil moisture datasets, particularly in such mountainous areas [12].

Over the past decades, acquisition of soil moisture data has evolved from traditional gravimetric methods to the applications of semi-automatic and automatic monitoring of the neutron probe, time-domain reflectometry (TDR), frequency domain reflectometry (FDR). At the regional scale, remote sensing, particularly satellites, provides soil moisture estimates over large areas [13], which is mainly based on the measurement of electromagnetic radiation energy reflected or emitted from the land surface. Satellite soil moisture products mainly include AMSR (Advanced Microwave Scanning Radiometer) [14], ERS (European Remote Sensing Satellite) [15], ASCAT (The Advanced Scatterometer) [16,17], SMOS (Soil Moisture and Ocean Salinity) [18] and SMAP (Soil Moisture Active Passive) [19]. In addition, soil moisture data at the regional scale can also be obtained through model simulation and data assimilation [20]. Common weaknesses of these soil moisture products are that the accuracy and resolution in heterogeneous mountainous areas are still too coarse to meet the study requirements [21,22]. Temperature Vegetation Dryness Index (TVDI) [23] and Apparent Thermal Inertia (ATI) [24,25] are two common methods to estimate soil moisture by using visible light and near-infrared wavebands. However, both the TVDI and ATI methods mainly establish the correlation between the measured soil moisture on the ground and the TVDI or ATI indices to estimate the soil moisture distribution in the region. For alpine and heterogeneous areas, the complexity of the underlying surface leads to a series of uncertainties, such as the inconsistent linear relationship between soil moisture and ATI, resulting in large estimation errors. In addition to these deficiencies, current remote sensing methods mainly concentrate on the relationship between the surface reflection value and the in situ observations to estimate the surface soil moisture at the regional scale [23]. Few studies have estimated the profile soil moisture, particularly in the alpine areas. Li et al. [26] used remotely sensed surface soil moisture to calculate deep soil moisture by a flux model, and pointed out that remote sensing surface soil moisture in wet areas was suitable for estimating profile soil moisture, while the results in dry areas had large errors. Tobin et al. [27] downscaled AMSR-E and ERS-CCI (European remote sensing satellite-climate change initiative) soil moisture data using an exponential filter (ExpF) with soil moisture index derived from MODIS NDVI. Tian et al. [3] coupled the surface soil moisture and profile soil moisture, applied ExpF, artificial neural networks (ANN) and cumulative distribution function matching (CDF) methods in an alpine region to estimate the deep profile soil moisture at the regional scale. Lu et al. [28] investigated a nonlinear autoregressive neural network method with exogenous input (NARXnn) to estimate time series soil moisture by multiple remote sensing data. Estimation of 0–100 cm soil moisture by the principle of maximum entropy achieved better results than those obtained by the exponential decaying function in the Southeastern USA, a subtropical humid area [29]. With the measurement of the spectral characteristics of soil profile, Balet et al. [30] inferred soil moisture conditions based on the MARMIT (MultiLayer Radiative Transfer Model for soil reflectance) model. Over the past decades, MODIS LST and NDVI products have been widely used in agriculture, ecosystem and global change research [31,32]. The NDVI is an index that shows the difference between vegetation reflectance in the visible and near-infrared bands and the soil background [33]. Land Surface Temperature (LST) is a key parameter for agricultural drought monitoring, hydrological research and urban thermal environment [34,35]. Both MODIS LST and NDVI data are widely used for soil moisture estimation based on the TVDI and ATI methods (e.g., [21,36]). For example, Yang et al. [37] proposed a trapezoidal space defined by remote sensed vegetation cover and LST to estimate surface soil moisture. Compared with the aforementioned soil moisture products, both MODIS LST and NDVI have higher

spatial resolutions in soil moisture monitoring. In addition, both MODIS LST and NDVI are usually used for downscaling the satellite soil moisture products [22,38].

In recent years, many scale transformation studies for soil moisture retrieval have been done. However, the accuracy of most of these works was poor in mountainous areas, and the temporal and spatial resolutions of profile soil moisture estimation were still too coarse to meet the needs of hydrological research in heterogeneous mountain areas. To improve the deficiency in estimating profile soil moisture distribution over mountainous areas, this study proposed a novel approach to estimate profile soil moisture by integrating remote sensing LST and NDVI products and in situ soil moisture observations. The upstream of the Heihe River Watershed in the Qilian Mountain Ranges in Northwest China was chosen as the study area to estimate the profile soil moisture (0–70 cm depth) at the regional scale by remote sensing. The study area was divided into 31 zones based on the combination of altitude, vegetation and soil type. In situ soil moisture observation stations were set up at each of the zones to collect soil moisture at five layers (0–10, 10–20, 20–30, 30–50 and 50–70 cm) continuously for the period of October, 2013 to September, 2016. Multiple time series MODIS NDVI, LST and soil moisture were fitted for each of the five soil layers at the 31 zones to estimate the profile soil moisture distribution on a regional scale. The study aims to provide a novel approach to estimate profile soil moisture distribution by remote sensing to support hydrological research in mountainous areas.

2. Study Area

The in situ soil moisture data for this study were obtained from the Soil Hydrological Heterogeneity Observation Network in the upstream of the Heihe River Watershed (97°46′–101°11′E, 38°12′–39°22′N) Northwest, China (Figure 1a), a $2.75 \times 104 \text{ km}^2$ study area with 30 tributaries, elevation ranging from 2000 m to 5580 m (above sea level, a.s.l) on the northeast edge of the Qinghai–Tibet Plateau. The spatial distribution of annual mean temperature ranges from $-3.1 \text{ }^\circ\text{C}$ to $3.6 \text{ }^\circ\text{C}$, and annual precipitation ranges from 200 mm to 700 mm [39]. Perennial snow cover and glaciers are present above 4000 m with permafrost extending down to 3700 m. Affected by mountain climate and terrain, there is a remarkable vertical zonal distribution of vegetation and soils in the study area. In the upstream of the Heihe River Watershed, the major vegetation types include coniferous forest (*Picea crassifolia*), shrub (*Potentilla fruticosa*), steppe (*Stipa purpurea* Griseb), alpine meadow (*Kobresia pygmaea* Clarke), alpine sparse vegetation (*Saussurea medusa* Maxim) and desert (*Sympegma regelii* Bunge) [22]. The main soil types include aeolian sandy soil, cold desert soil, alpine meadow soil and mountain swamp chestnut soil [8].

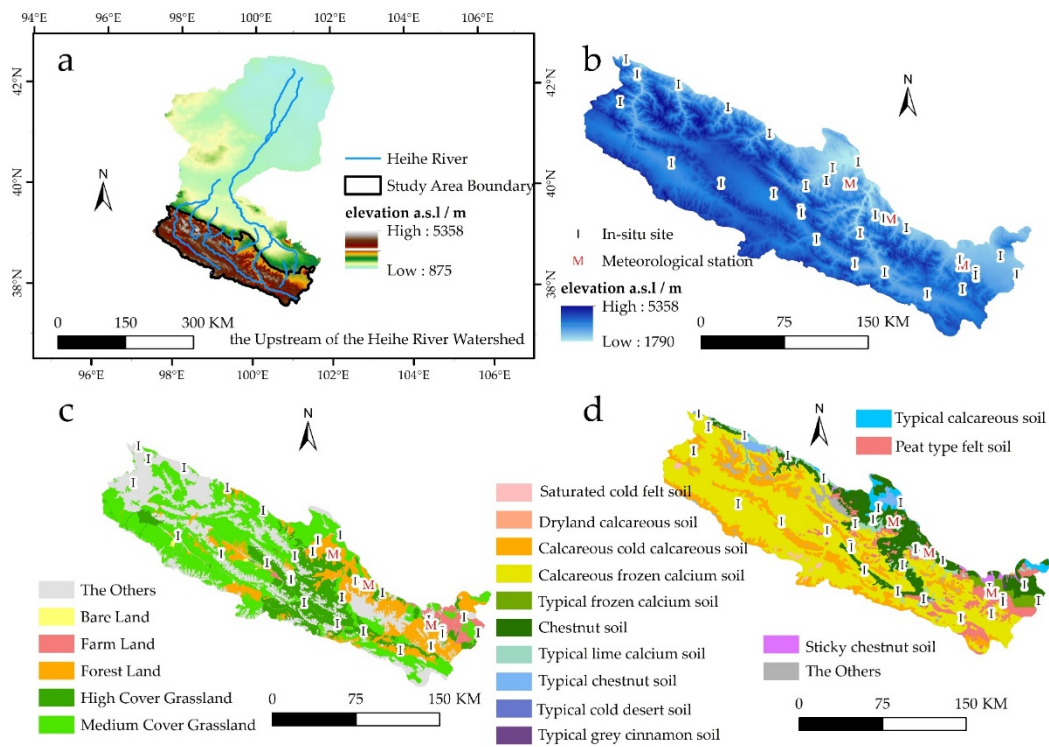


Figure 1. The in situ observation stations in the upstream of the Heihe River Watershed, Northwest China. The number shows 31 land use/land cover (LULC) soil elevation types (details in Table 1). (a) the study area in China; (b) the elevation of the study area, black circles represent the in situ sites and crimson circles represent the three automatic meteorological station sites; (c) land use types distribution in the study area; (d) soil types. The locations of in situ monitoring sites and meteorological stations are also indicated in (b), (c) and (d).

Table 1. Soil and vegetation types at the in situ observation sites and automatic meteorological stations.

ID	Elevation Range (m)	Soil Type	Vegetation Type	Percent (%) of Area
No.1	2000–2500	Typical lime calcium soil	Medium coverage grassland	1.53
No.2	2000–2500	Chestnut soil	Medium coverage grassland	0.91
No.3	2000–2500	Sticky chestnut soil	Medium coverage grassland	1.34
No.4	2500–3000	Typical chestnut soil	Medium coverage grassland	3.06
No.5	2500–3000	Chestnut soil	Medium coverage grassland	2.87
No.6	3000–3500	Chestnut soil	Medium coverage grassland	0.96
No.7	3000–3500	Calcareous frozen calcium soil	Medium coverage grassland	2.48
No.8	3000–3500	Saturated cold felt soil	Medium coverage grassland	3.79
No.9	3500–4000	Saturated cold felt soil	Medium coverage grassland	7.57
No.10	3500–4000	Calcareous frozen calcium soil	Medium coverage grassland	5.47
No.11	2500–3000	Typical chestnut soil	Forest land	3.22
No.12	2500–3000	Typical gray cinnamon soil	Forest land	1.34
No.13	2500–3000	Peat type felt soil	Forest land	0.97
No.14	2500–3000	Chestnut soil	Forest land	1.63
No.15	3000–3500	Peat type felt soil	Forest land	2.77
No.16	3000–3500	Saturated cold felt soil	Forest land	2.62
No.17	3500–4000	Peat type felt soil	Forest land	1.02
No.18	2500–3000	Typical calcareous soil	Farm land	2.05
No.19	2500–3000	Dryland calcareous soil	Farm land	1.66
No.20	2500–3000	Calcareous cold calcareous soil	Bare land	1.31
No.21	3000–3500	Calcareous cold calcareous soil	Bare land	1.74
No.22	3000–3500	Saturated cold felt soil	Bare land	1.04
No.23	3500–4000	Typical frozen calcium soil	Bare land	1.48
No.24	4000–4500	Typical cold desert soil	Bare land	9.33
No.25	4000–4500	Saturated cold felt soil	Bare land	3.54
No.26	2500–3000	Typical chestnut soil	High coverage grassland	1.24
No.27	2500–3000	Chestnut soil	High coverage grassland	1.01
No.28	3000–3500	Typical chestnut soil	High coverage grassland	2.40
No.29	3000–3500	Peat type felt soil	High coverage grassland	1.54
No.30	3000–3500	Saturated cold felt soil	High coverage grassland	3.73
No.31	3500–4000	Saturated cold felt soil	High coverage grassland	7.02
Biandukou	3000–3500	Peat type felt soil	High coverage grassland	
Kangle	2000–2500	Chestnut soil	Medium coverage grassland	
Dayekou	2500–3000	Chestnut soil	Forest land	

3. Data Sets

3.1. In Situ Soil Moisture Monitoring Network

3.1.1. Soil Moisture Observation Network

We established a Soil Hydrological Heterogeneity Observation Network comprising 31 stations (Figure 1) in the upstream of the Heihe River Watershed based on the combination of land use/land cover (LULC), soil type and elevation [39,40]. The distribution of soil and vegetation types is shown in Table 1. We used GPS (Garmin Oregon 550) to record latitude, longitude and altitude information for each station, the positional errors were within ± 1 m and altitude error was in ± 3 –5 m. We also recorded soil profile characteristics, vegetation status, root depth, aspect and slope using a geological compass, and took pictures of the sites every summer since June, 2014.

3.1.2. Soil Moisture Measurement

ECH2O 5TE soil moisture probes (DECAGON Devices, USA) and EM50 datalogger were installed at each in situ observation site. The 5TE probe measures the soil volumetric water content by the dielectric constant of the soil, with a precision of $\pm 3\%$ and accuracy of ± 1 –2% [3,41]. The 5TE probes with a sensing depth of 2.5 cm were vertically centered in each of the sampled layers (0–10 cm, 10–20 cm, 20–30 cm, 30–50 cm and 50–70 cm) [42]. There is one probe in each layer for a total of five at each station. Datalogger EM50 was placed into a waterproof box sealed with high-strength glass glue and wrapped in a thick waterproof bag buried at a distance of at least 50 cm away from the 5TE probes. The system collected soil moisture content data at 30 min intervals. Regular site maintenance took place twice a year at the beginning of June and at the end of October [3].

However, the mountainous study area is topographically complex and hard to reach, and it is a real challenge to maintain the soil moisture in situ observation network in the study area. Wireless data transmission is not possible because there is no mobile communication network coverage in the study area. As a result, there are some gaps in the measurement datasets due to severe weather and unstable batteries or sensors and the sensor damage by livestock and rats [3].

3.2. Time Series Data of NDVI and LST

NDVI was used as the vegetation index for the upscaling of the in situ soil moisture in this study. Specifically, we acquired the 16-day composite NDVI dataset MOD13A2 V6 (<https://e4ftl01.cr.usgs.gov/MOLT/MOD13A2.006/>) of the sixth edition of terrestrial Level 3 standard data products for the period of October, 2013 to September, 2016, with a total of 69 scenes at a spatial resolution of 1 km² [43]. We used the 8-d composite Land Surface Temperature (LST) data MOD11A2 V6 (<https://e4ftl01.cr.usgs.gov/MOLT/MOD11A2.006/>) for the same period of October, 2013 to September, 2016, for a total of 138 scenes with a resolution of 1 km² [44]. Since the LST data were of 8-d composite, we used Maximum Value Composites (MVC) to process the LST dataset into a 16-d temporal resolution to match the temporal frequency of the NDVI dataset [45].

4. Methodology

The remote sensing vegetation index products contain a lot of noise caused by precipitation, cloud cover, human influence and the sensor itself in the data acquisition and process stages [46,47], and these factors can be collectively called random factors or residual parts.

The MOD13A2 V5 NDVI product was divided into the NDVI seasonal part and the NDVI residual part by using the Asymmetric Gaussian fitting method (AG) [48]. The multivariate linear regression fitting was used to establish multiple linear regression equations between the time series soil moisture data and the MODIS LST and NDVI. Subsequently, soil moisture upscaling equations were developed for every profile in the 31 vegetation–soil–elevation zones.

We installed only three automatic weather stations in the study region due to resource constraints. The limited number of precipitation observation stations cannot match the number of in situ soil moisture observations. Our in situ observations covered the three-year period (October, 2013 to September, 2016), and were able to represent the mean precipitation amount in the study region. Therefore, we only used MODIS LST and NDVI remote sensing data to estimate the spatial distribution of soil moisture in the study region.

4.1. Asymmetric Gaussian Function Fitting

Based on the noise information, NDVI data products can be divided into seasonal part, NDVI_{AG}, and residual part, NDVI_{RES} as shown in Equation (1). It needs to be reconstructed to remove the residual part [48].

$$\text{NDVI} = \text{NDVI}_{\text{AG}} + \text{NDVI}_{\text{RES}} \quad (1)$$

The time series NDVI data curve reconstructed by the AG algorithm, can well express the interannual variation characteristics of the vegetation, and identify all the abnormal values [31]. The AG algorithm is a nonlinear least-squares fitting algorithm based on the Asymmetric Gaussian function. The original NDVI data and NDVI_{AG} were used to obtain the residual part of the time series Vegetation Index (NDVI_{RES}). The shallow soil moisture was greatly affected by the residual part which was likely to be related to short-term weather. The deep soil moisture was mainly subject to the seasonal changes in weather conditions and plant growth and environmental factors.

4.2. Multiple Linear Regression Fittings

In this study, a multiple linear regression method was used to estimate the soil moisture using the in situ soil moisture observations, Vegetation Index (NDVI) and Land Surface Temperature (LST) data. The specific equation is as follows:

$$SMC = a_0 + a_1 * LST + a_2 * NDVI_{RES} + a_3 * NDVI_{AG} \quad (2)$$

In Equation (2), SMC is soil volumetric water content ($m^3 m^{-3}$), LST is the Land Surface Temperature (K), $NDVI_{RES}$ and $NDVI_{AG}$ are the residual part and seasonal part of the vegetation index, respectively, a_0 , a_1 , a_2 and a_3 are the coefficients to be determined, a_1 is in $m^3 m^{-3} K^{-1}$, while a_2 and a_3 are dimensionless.

Following Zhang et al. [22], the regression equations were evaluated by complex correlation coefficient (R), the F-test value, the confidence level P and the root mean square error (RMSE). R describes the linear correlation of the dependent variable (soil moisture) and multiple explanatory variables in multivariate linear regression. The F-test was used to test whether the established regression equation is statistically significant. The larger the F-value, the better the fitted regression equation. Confidence level P indicated the significance level of the regression equation. The smaller the p -value, the more significant the equation. RMSE was used to measure the deviation between the predicted value and the true value. The smaller the RMSE value, the closer the simulated value to the observed value, the higher the accuracy of the regression equation. R and RMSE calculation formulas are as follows:

$$R = \frac{\sum_{i=1}^n (SMC_{obs,i} - \overline{SMC}_{obs})(SMC_{mod,i} - \overline{SMC}_{mod})}{\sqrt{\sum_{i=1}^n (SMC_{obs,i} - \overline{SMC}_{obs})^2} \sqrt{\sum_{i=1}^n (SMC_{mod,i} - \overline{SMC}_{mod})^2}} \quad (3)$$

$$RMSE = \sqrt{\frac{\sum_{i=1}^n (SMC_{obs,i} - SMC_{mod,i})^2}{n}} \quad (4)$$

where, $SMC_{obs,i}$ is the measured soil moisture value, $SMC_{mod,i}$ is the multiple linear regression fitted soil moisture value, n is the number of observations [22].

5. Results and Discussions

5.1. Time Series NDVI and LST

The NDVI dataset was the MOD13A2 product from 16 October 2013 to 29 September 2016. The product was the 16-day composite with a total of 69 images. $NDVI_{AG}$ (Figure 2b) was obtained by reconstructing the NDVI time series data with the AG algorithm, and then the $NDVI_{AG}$ and the original NDVI data (Figure 2a) were used to derive the residual $NDVI_{RES}$ (Figure 2c). The reconstructed NDVI time series data ($NDVI_{AG}$) based on the AG algorithm and the trend of the original NDVI time series data were basically the same (Figure 2d), and the reconstructed results were used to detect abnormally high and low values in the time series data, to correct the low values, and to reflect seasonal changes in the vegetation index [49]. The seasonal $NDVI_{AG}$ and the residual $NDVI_{RES}$ were consistent with the growth pattern of the vegetation [48].

The selected LST dataset was the MOD11A2 product from 16 October 2013 to 29 September 2016, which was an eight-day composite product with a total of 138 images. The eight-day LST dataset was converted to a 16-day LST images (Figure 3b) to match the NDVI temporal resolution by the MVC method [45].

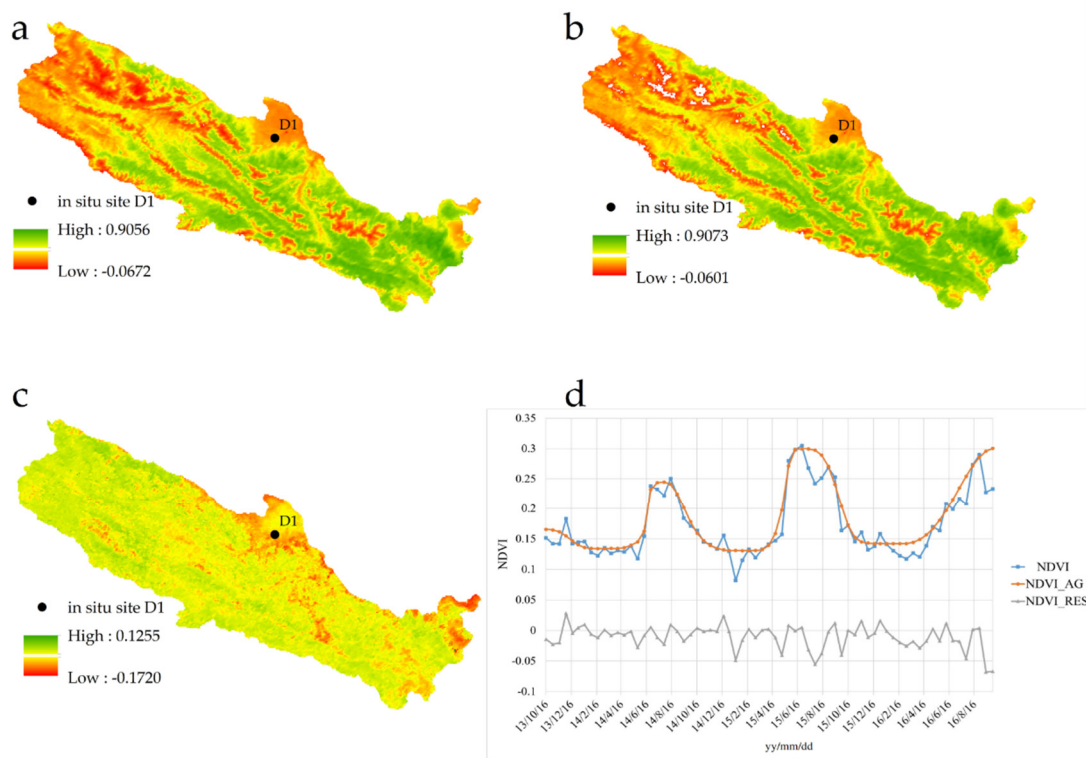


Figure 2. Vegetation Index (NDVI) in the study area. (a) The NDVI distribution and the location of the in situ observation site D1; (b) the $NDVI_{AG}$ distribution; (c) the $NDVI_{RES}$ distribution; (d) the $NDVI/NDVI_{AG}/NDVI_{RES}$ change at the site D1.

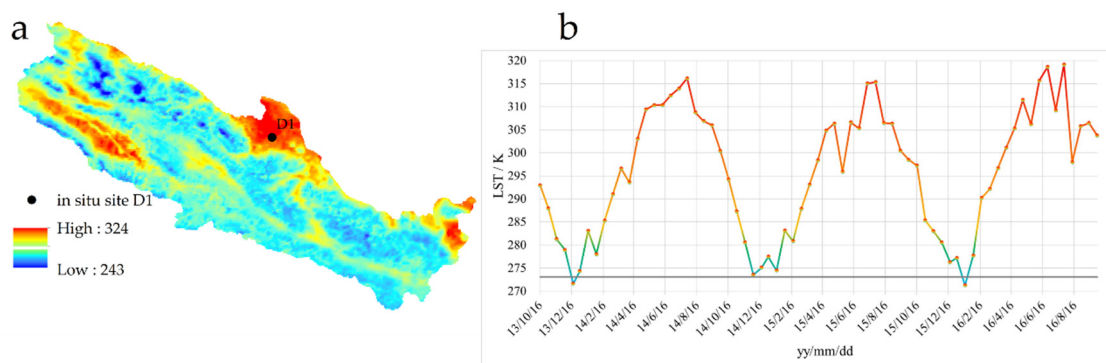


Figure 3. Land Surface Temperature (LST) data in the study area. (a) the LST distribution and the location of the in situ observation site D1; (b) the LST change at the site D1. The temperature is in Kelvin.

5.2. Upscaling of In Situ Soil Moisture

The soil moisture time series data in the 31 in situ observation sites were processed to 16-day mean values corresponding to the NDVI and LST's temporal resolution. Subsequently, multiple linear regressions were established between the in situ soil moisture observations and the NDVI and LST time series data. The five-layer soil moisture upscaling equation coefficients of the 31 in situ observation sites were shown in Tables 2 and A1, Tables A2–A4. For the 0–10 cm layer of the site D8, the soil moisture upscaling equation was significant at a 95% confidence level, and all the other models at the rest 31 in situ observation sites were significant at a 99% level. Among them, the correlation coefficient R of the 0–10 cm layer was 0.36–0.93, the RMSE was 0.03 (Table 2); the R and RMSE of 10–20 cm layer were 0.65–0.90, and 0.03 (Table A1), respectively; The R and RMSE of 20–30 cm layer were 0.51–0.95 and 0.03 (Table A2), respectively; the R and RMSE of 30–50 cm layer were 0.47–0.93, and 0.03 (Table A3),

respectively; and the R and RMSE of 50–70 cm layer were 0.54–0.94, and 0.02, respectively (Table A4). The accuracy of scaling results was higher than that of Xu et al. [21]. In general, the five-layer RMSE mean values were close to the ECH2O data accuracy ($0.03 \text{ cm}^3 \text{ cm}^{-3}$), indicating that the accuracy of the in situ soil moisture estimation models was reasonable.

Table 2. Layer soil moisture estimation model (0–10 cm).

Site	Intercept- a_0	LST- a_1	NDVI _{RES} - a_2	NDVI _{AG} - a_3	F-Value	R	RMSE
D1	−0.1428	0.0006	0.4888	0.3638	27.1860 **	0.7564	0.0230
D2	0.1053	−0.0003	0.1883	0.1883	42.9037 **	0.8151	0.0156
D3	−0.0943	0.0004	0.5355	0.2924	9.1448 **	0.5448	0.0264
D4	−0.1903	0.0008	0.3047	0.0796	21.4239 **	0.7051	0.0184
D5	−0.3828	0.0017	0.0371	0.1482	24.7216 **	0.7300	0.0402
D6	−0.2111	0.0009	−0.0079	0.1728	13.7290 **	0.6721	0.0374
D7	−0.1888	0.0007	0.1290	0.2629	41.9671 **	0.8121	0.0224
D8	−0.1269	0.0006	0.1196	0.0833	3.2826 *	0.3627	0.0348
D9	−0.2464	0.0012	−0.1120	0.1672	28.5156 **	0.7538	0.0384
D10	−0.2147	0.0006	0.3632	0.6959	44.2519 **	0.8193	0.0278
D11	−0.1179	0.0003	0.2781	0.2624	44.5027 **	0.8201	0.0316
D12	−0.5345	0.0021	0.1640	0.1196	24.0405 **	0.8130	0.0284
D13	−1.3622	0.0055	−0.1438	0.0452	26.5764 **	0.7422	0.0693
D14	−0.7388	0.0028	−0.2080	0.0848	30.9407**	0.8456	0.0284
D15	−3.7797	0.0144	−0.4288	−0.1371	34.2043 **	0.7824	0.0986
D16	−0.4971	0.0021	0.0441	0.0946	40.0270 **	0.8055	0.0294
D17	−0.8997	0.0035	0.0051	0.3303	49.3673 **	0.8780	0.0464
D18	−0.8674	0.0032	−0.1961	0.0720	20.9669 **	0.7243	0.0426
D19	−0.4460	0.0020	−0.0038	0.0830	37.9425 **	0.7978	0.0313
D20	−0.0336	0.0002	0.0248	0.2648	14.7577 **	0.6579	0.0326
D21	−0.0005	−0.0001	0.4719	0.8539	18.8724 **	0.7122	0.0208
D22	−0.0523	0.0003	0.1973	0.2839	13.0625 **	0.6133	0.0183
D23	−0.9314	0.0034	0.0434	0.2500	69.0881 **	0.8725	0.0308
D24	−0.1344	0.0005	0.1318	0.2409	91.0531 **	0.9325	0.0194
D25	−0.3850	0.0016	0.3814	0.2454	46.1557 **	0.8249	0.0271
D26	−0.3739	0.0017	0.5105	0.1177	31.1755 **	0.7681	0.0319
D27	−0.4618	0.0019	0.1124	0.0800	18.9346 **	0.6829	0.0352
D28	−0.4352	0.0021	0.1503	0.1258	118.7521 **	0.9229	0.0175
D29	−0.9221	0.0038	−0.0596	0.1164	55.6932 **	0.8713	0.0366
D30	−0.6680	0.0028	0.1740	0.1285	44.6734 **	0.8269	0.0290
D31	−0.9122	0.0033	0.0739	0.3898	56.3416 **	0.8517	0.0589

* and ** represent F-test significance level of 95% and 99%, respectively. The table keeps 4 decimal places, the calculation keeps 8 decimal places. Intercept- a_0 , LST- a_1 , NDVI_{RES}- a_2 and NDVI_{AG}- a_3 represent the coefficients of upscaling Equation (2). F-value means the significance value in the F-test. R is the complex correlation coefficient. RMSE is the root mean square error.

The soil moisture of each pixel (with spatial resolution of 1 km^2) at the 31 zones from 16 October 2013 to 29 September 2016 was calculated by using the upscaling model to obtain the five-layer soil moisture dataset in the study area for the same study period. The dataset covered an area of $2.75 \times 10^4 \text{ km}^2$, with a temporal resolution of 16-day and a spatial resolution of 1 km^2 (e.g., Figure 5).

5.3. Accuracy Evaluation of Upscaling Soil Moisture Models

To evaluate the accuracy of soil moisture upscaling models, the three sites—Biandukou, Dayekou and Kangle, which were not used to establish the regression equations, were used as validation sites, and their soil moisture data were used for correlation test and error analysis (Table 3). The results of the soil moisture upscaling in the different soil layers showed that the correlation coefficients were between 0.5410 and 0.8940, and the RMSE were between 0.0066 and 0.0549, all of which passed the F-test at 99% significant level. The results showed that the correlation between the upscaled data and

the measured data were significant, and the soil moisture upscaling models well expressed the dry and wet conditions of the soil at the regional scale.

Table 3. Verification of the soil moisture upscaling equations at the three in situ observation sites.

Layer	Site	N	R	RMSE	F-Value
0–10 cm	Biandukou	48	0.6645	0.0373	36.3749 **
	Dayekou	54	0.7247	0.0417	57.5060 **
	Kangle	54	0.6766	0.0247	43.9005 **
	mean		0.6886	0.0346	45.9271 **
10–20 cm	Biandukou	55	0.7366	0.0255	62.8749 **
	Dayekou	54	0.6310	0.0549	34.4064 **
	Kangle	49	0.7981	0.0127	82.4391 **
	mean		0.7219	0.0310	59.9068 **
20–30 cm	Biandukou	55	0.7172	0.0258	56.1386 **
	Dayekou	54	0.7455	0.0275	65.0525 **
	Kangle	54	0.8376	0.0106	122.2273 **
	mean		0.7668	0.0213	81.1394 **
30–50 cm	Biandukou	55	0.5410	0.0339	21.9261 **
	Dayekou	54	0.5908	0.0342	27.8885 **
	Kangle	53	0.8940	0.0066	203.0996 **
	mean		0.6753	0.0249	84.3048 **
50–70 cm	Biandukou	30	0.5254	0.0338	10.6759 **
	Dayekou	54	0.6441	0.0247	36.8675 **
	Kangle	54	0.8187	0.0094	105.6833 **
	mean		0.6627	0.0226	51.0756 **
total	Biandukou		0.6369	0.0313	37.5981 **
	Dayekou		0.6672	0.0366	44.3442 **
	Kangle		0.8050	0.0128	111.4700 **

** means F-test at 99% significance. N is the observations.

Comparing the validation results of soil moisture models of the five layers, we found that the R's descending order was 20–30 cm > 10–20 cm > 0–10 cm > 30–50 cm > 50–70 cm, RMSE's descending order was 0–10 cm > 10–20 cm > 30–50 cm > 50–70 cm > 20–30 cm. The trends of the two indices were not consistent, the main reason might be: 1) the variability of soil moisture with time decreased from the top to the bottom soil layer, and the 0–10 cm layer had the largest soil water fluctuation and the largest error, 2) the LST was mainly affected by the 0–10 cm layer of soil and overlying vegetation, 3) NDVI was mainly affected by the vegetation growth, and the root zone soil moisture was very important for vegetation growth, the main vegetation types of the three verification sites were all grassland, with their root system mainly distributed in the 20–30 cm. Therefore, the accuracy of the 20–30 cm soil moisture upscaling model was the highest, and the lowest was the 50–70 cm layer.

Comparison of the soil moisture upscaling results of the three verification sites showed that the RMSE values were getting smaller from the top to the deep soil layers, Kangle appeared to have the best fit. Topographically, the Kangle site was located at a plateau within 1 km² pixels. The vegetation type was mainly grass (*Stipa* Steppe) with homogeneous distribution. The climate was dry, with smaller rainfall (annual 338 mm for Kangle, 428 mm for Dayekou and 702 mm for Biandukou during the 2013–2016 period), the soil moisture was relatively low and stable. Under these climate, topography and vegetation conditions, the LST and NDVI data were of relatively high quality, and the accuracy of the upscaling was high. The Biandukou and Dayekou sites were located on the mountain slope. The terrain was complex within 1 km² pixels, and the vegetation types were diverse. In addition, there was a reservoir near the Dayekou site. These factors were likely to have affected the LST and NDVI quality of remote sensing products, and the accuracy of the upscaling model was not as good as that of the *Kangle* site.

5.4. Soil Moisture Variability at Different Temporal and Spatial Scales

5.4.1. Temporal Variability of Soil Moisture at the Regional Scale

Figure 4 shows the changes in soil moisture at different layers over time. As Figure 4a shows, the soil moisture was the lowest in December and the highest in July. The descending soil moisture order in all the layers in December were 20–30 cm > 50–70 cm > 10–20 cm > 30–50 cm > 0–10 cm. The descending soil moisture order in all the layers in July were 20–30 cm > 10–20 cm > 0–10 cm > 30–50 cm > 50–70 cm. Among them, the 20–30 cm were the highest among all the layers of the soil profile. During the whole three years, the variation range of each layer was 0–10 cm (coefficient of variation, CV. 12.44%), 10–20 cm (CV. 12.27%), 20–30 cm (CV. 11.86%), 30–50 cm (CV. 10.40%), 50–70 cm (CV. 8.38%), respectively, which was closely related to the effects of precipitation and soil infiltration on soil moisture. Figure 4b shows that the 20–30 cm and 30–50 cm had a relatively high and low but stable variation. Among the four seasons, the precipitation and temperature were low in winter, leading to the decrease of liquid water in the soil, thus the soil moisture was the lowest in the winter. Summer rainfall was the highest and most frequent, therefore the soil moisture content was highest and most variable in the summer.

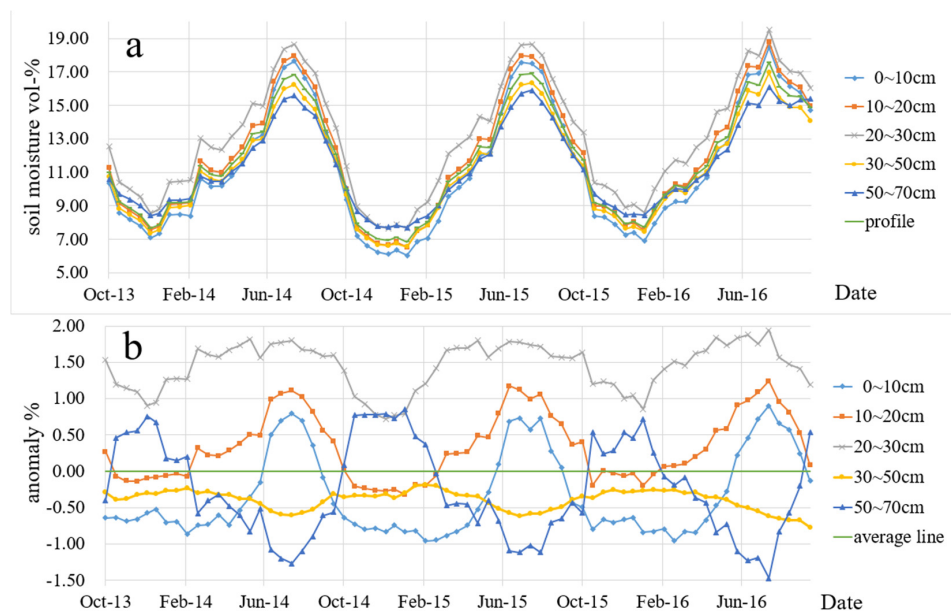


Figure 4. Temporal variability of soil moisture. (a) temporal variability of soil moisture in real value; (b) anomaly between each layer and the mean soil moisture.

5.4.2. Spatial Distribution of Soil Moisture at the Regional Scale

The overall spatial distribution of soil moisture during the growing season from 2014 to 2016 are shown in Figure 5. The weighted mean soil moisture of the three years was 14.50% in the entire study region. Soil moisture was higher in most of the eastern, central and northwestern parts of the region. Overall, the soil moisture in the eastern area was generally higher than that in the central and western areas, and the soil moisture was the lowest in the western area. The spatial patterns were consistent with the precipitation distribution pattern shown in Figure 5d and Tian et al. [42]. The precipitation during the growth period of 2014 to 2016 was highest in the Biandukou, the second highest in the Dayekou, and the lowest in the Kangle automatic weather station, showing a spatial pattern of a declining trend from the eastern to the central and to the western parts of the region. Since the limited number of automatic weather stations and coarse spatial coverage, the precipitation was not incorporated into the regression analysis.

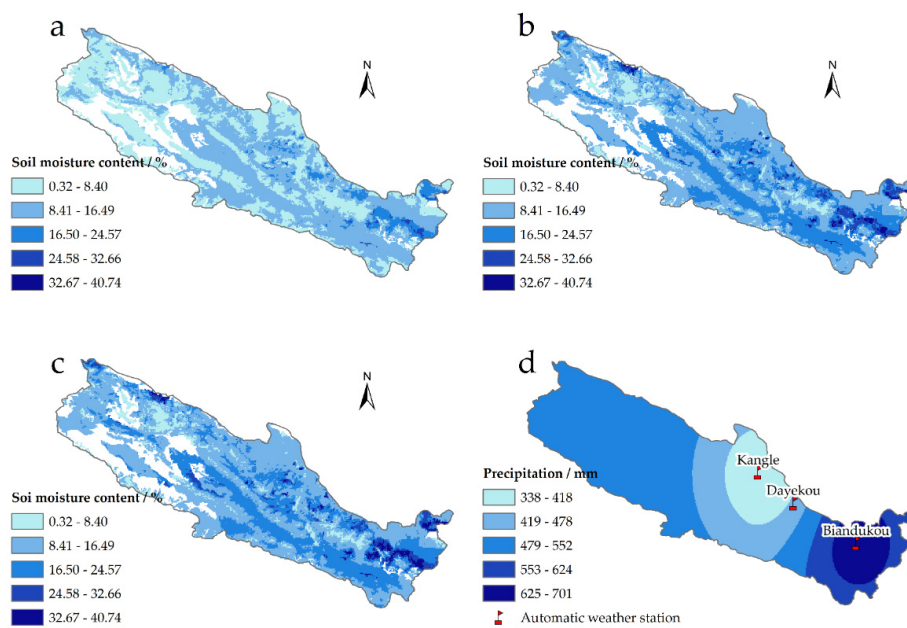


Figure 5. Spatial distribution of soil moisture during the 2014–2016 growth period. (a) 2014 growth period; (b) 2015 growth period; (c) 2016 growth period; (d) rainfall distribution pattern by kriging interpolation based on data obtained from the three automatic weather stations during the 2014–2016 period.

5.4.3. Soil Profile Moisture Heterogeneity at the Regional Scale

As shown in Figure 6, soil moisture and its variability at different layers were shown by the relationship between the mean and coefficient of variation (CV). The fitting curves indicated that the variability of soil moisture at the shallow layers was larger than deeper layers. Mean and CV had negative correlations in the 30–50 cm and 50–70 cm layers, indicating that the soil moisture variability was the highest in dry conditions and the lowest in humid conditions (e.g., summer), and the fitting curve between the 30–50 cm layers and the whole profile was close, indicating that the characteristics of the soil moisture change in the 30–50 cm was similar to that of the whole profile. As described in the above section, the most representative of the whole profile was 30–50 cm among the five layers.

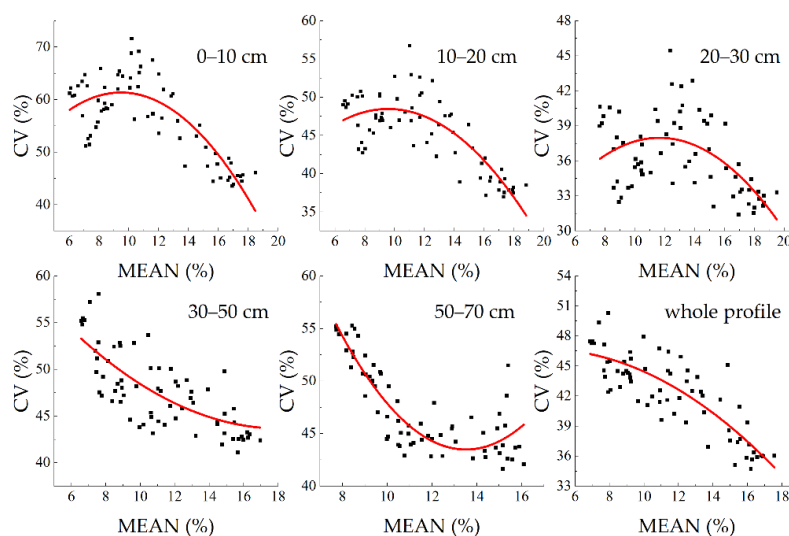


Figure 6. Mean and coefficient of variation (CV) of soil moisture at different layers.

6. Conclusions

Estimating spatial and temporal distribution of soil moisture is a challenge in high-elevation, data-scarce, and heterogeneous mountainous areas like the upstream of the Heihe River Watershed in Northwest China. We proposed a regression model based on the MODIS NDVI and LST to estimate profile soil moisture at the regional scale. Subsequently, we analyzed the spatial and temporal variability of soil moisture at the regional scale. Results showed that the multivariate linear regression method could be used to estimate high-resolution soil moisture products in alpine and cold mountainous areas at both shallow and deep soil layers. The soil moisture in the east of the upstream of the Heihe River Watershed was significantly higher than that in the west, and the average soil moisture in the whole region was 14.5% in the 0–70 cm depth. The soil moisture at the 30–50 cm soil layer could reasonably represent the 0–70 cm profile soil moisture. Soil moisture in the 0–10 cm layer had the highest variability while the 20–30 cm layer showed the lowest soil moisture variability among all the layers. The contribution of this study was to estimate profile soil moisture at the regional scale by readily available remote sensing products of NDVI and LST.

However, the microterrain features such as slope and aspect were not considered in the soil-vegetation-elevation sampling zone, which might affect the accuracy of soil moisture upscaling models. Satellite products with high spatial-temporal resolutions need to be integrated with in situ observations and other soil and vegetation datasets to improve the accuracy of estimating soil moisture at the regional scale, especially in data-scarce and topographically complex mountainous regions.

Author Contributions: Conceptualization, X.B., L.Z. and C.H.; field work: X.B. and Y.Z.; processing and analysis, X.B. and L.Z.; writing—original draft preparation, X.B. and L.Z.; review, editing, and finalization, C.H.; project administration, C.H. All authors have read and agreed to the published version of the manuscript.

Funding: The project is partially funded by the grants from National Natural Science Foundation of China (41530752, 41877148, 41501016 and 91125010).

Acknowledgments: We are grateful to the members of the Center for Dryland Water Resources Research and Watershed Science, Lanzhou University for their hard field work to collect and analyze the soil data in the high and cold, hard to reach mountainous areas over the past seven years. Meanwhile, we are deeply grateful to the anonymous reviewers and Section Managing Editor Muriel Zhang for their constructive comments and responsible work.

Conflicts of Interest: The authors declare no conflict of interest.

Appendix A

Table A1. Layer soil moisture estimation model (10–20 cm).

Site	Intercept- a_0	LST- a_1	NDVI _{RES} - a_2	NDVI _{AG} - a_3	F-Value	R	RMSE
D1	−0.0448	0.0003	0.1239	0.1552	47.1598 **	0.8359	0.0082
D2	0.0356	0.0000	0.1810	0.1748	38.1284 **	0.7985	0.0170
D3	−0.2269	0.0008	0.4974	0.6081	45.2227 **	0.8222	0.0224
D4	−0.1502	0.0007	0.0725	0.0469	62.7791 **	0.8798	0.0079
D5	−0.4594	0.0020	−0.0527	0.0761	25.6997 **	0.7366	0.0294
D6	−0.1641	0.0008	−0.0593	0.1495	12.7288 **	0.6580	0.0351
D7	−0.0033	0.0000	0.2733	0.4083	44.2384 **	0.8193	0.0271
D8	−0.3441	0.0015	0.2253	0.2215	37.5842 **	0.7964	0.0256
D9	−0.3716	0.0016	0.0603	0.1356	41.7135 **	0.8113	0.0313
D10	−0.3128	0.0012	0.2242	0.4499	61.1032 **	0.8592	0.0204
D11	−0.0782	0.0003	0.2959	0.2660	60.4343 **	0.8580	0.0276
D12	−0.5718	0.0022	0.1828	0.0993	26.5246 **	0.8262	0.0266
D13	−0.6246	0.0028	−0.2230	0.1037	25.5179 **	0.7354	0.0561
D14	−0.7640	0.0030	−0.3891	0.0782	21.1450 **	0.7947	0.0345
D15	−3.1465	0.0121	−0.3682	−0.1379	49.6064 **	0.8343	0.0655
D16	−0.5756	0.0025	−0.0085	0.1084	31.9732 **	0.7721	0.0388
D17	−0.6236	0.0024	−0.0017	0.4309	38.3976 **	0.8507	0.0587
D18	−0.6764	0.0027	−0.1042	0.0408	22.3538 **	0.7126	0.0330
D19	−0.4705	0.0020	−0.0212	0.0813	36.9206 **	0.7938	0.0313
D20	0.0072	0.0001	0.0309	0.2423	18.7568 **	0.7017	0.0256
D21	0.0465	−0.0003	0.2537	0.9154	19.9186 **	0.7216	0.0205
D22	−0.0461	0.0002	0.1433	0.4214	33.0572 **	0.7772	0.0153
D23	−0.8592	0.0032	0.0515	0.2168	68.1222 **	0.8710	0.0283
D24	0.0002	0.0000	0.0661	0.1138	18.7331 **	0.7604	0.0185
D25	−0.4217	0.0018	0.3830	0.1929	49.7008 **	0.8345	0.0243
D26	−0.4072	0.0017	0.5010	0.1211	37.0421 **	0.7943	0.0300
D27	−0.4132	0.0016	0.0655	0.0041	15.6931 **	0.6481	0.0243
D28	−0.3328	0.0016	0.2332	0.1694	66.8502 **	0.8740	0.0250
D29	−1.4304	0.0057	−0.1453	0.0258	37.4054 **	0.8241	0.0436
D30	−0.7721	0.0031	0.1355	0.0902	50.5135 **	0.8366	0.0265
D31	−0.8850	0.0034	0.0180	0.1557	95.4179 **	0.9040	0.0253

** represents F-test significance level of 99%. The table keeps 4 decimal places, the calculation keeps 8 decimal places Intercept- a_0 , LST- a_1 , NDVI_{RES}- a_2 and NDVI_{AG}- a_3 represents the coefficients of upscaling Equation (2). F-value means the significance value in the F-test. R is the complex correlation coefficient. RMSE is the root mean square error.

Table A2. Layer soil moisture estimation model (20–30 cm).

Site	Intercept- a_0	LST- a_1	NDVI _{RES} - a_2	NDVI _{AG} - a_3	F-Value	R	RMSE
D1	-0.0083	0.0002	0.0743	0.2354	41.1005 **	0.8224	0.0111
D2	-0.1153	0.0007	0.0931	0.1193	34.1421 **	0.7822	0.0172
D3	-0.0706	0.0004	0.0280	0.1362	106.4698 **	0.9115	0.0045
D4	-0.1461	0.0007	0.0442	0.0442	81.4475 **	0.9158	0.0058
D5	-0.4863	0.0021	-0.0769	0.0640	42.4492 **	0.8137	0.0223
D6	-0.1669	0.0008	-0.0583	0.1072	10.6971 **	0.6252	0.0315
D7	-0.1960	0.0009	0.1118	0.2254	68.0018 **	0.8791	0.0164
D8	-0.2864	0.0013	0.2385	0.2561	73.0847 **	0.8783	0.0181
D9	-0.3968	0.0018	0.0137	0.0914	35.6686 **	0.7887	0.0300
D10	-0.1977	0.0009	0.1481	0.4672	97.0527 **	0.9042	0.0148
D11	-0.2159	0.0009	0.2404	0.2235	76.6659 **	0.8830	0.0230
D12	-0.4539	0.0019	0.1899	0.0817	30.0917 **	0.8422	0.0211
D13	-0.6281	0.0028	-0.2828	0.1395	20.4940 **	0.6972	0.0736
D14	-1.2032	0.0047	-0.5466	0.1281	28.3354 **	0.8347	0.0474
D15	-2.9820	0.0116	-0.3259	-0.1956	28.7933 **	0.7554	0.0724
D16	-0.5306	0.0023	-0.0735	0.0654	15.8860 **	0.6504	0.0431
D17	-0.4574	0.0019	0.1621	0.3431	36.6091 **	0.8450	0.0467
D18	-0.4233	0.0018	-0.1834	0.0218	7.6475 **	0.5108	0.0373
D19	-0.4601	0.0019	-0.0253	0.0735	40.5132 **	0.8072	0.0280
D20	0.0795	-0.0001	0.1087	0.2177	25.5517 **	0.7545	0.0182
D21	0.0384	-0.0002	0.1139	0.8839	25.9263 **	0.7654	0.0180
D22	-0.0273	0.0002	0.1510	0.3218	15.9146 **	0.6596	0.0162
D23	-0.8016	0.0032	0.0669	0.1044	77.8980 **	0.8845	0.0212
D24	-0.2004	0.0007	0.0031	0.0648	137.3034 **	0.9537	0.0058
D25	-0.4723	0.0019	0.4172	0.1751	47.0887 **	0.8462	0.0224
D26	-0.4483	0.0020	0.4454	0.0871	35.3780 **	0.7875	0.0288
D27	-0.2725	0.0011	0.0413	0.0380	23.8688 **	0.7240	0.0174
D28	-0.3072	0.0015	0.1535	0.1483	78.3862 **	0.8896	0.0207
D29	-1.7187	0.0068	-0.2184	0.0185	30.9722 **	0.7980	0.0554
D30	-0.7217	0.0029	0.1286	0.0932	48.8410 **	0.8323	0.0261
D31	-0.9337	0.0034	-0.0136	0.1848	51.1559 **	0.8401	0.0385

** represents F-test significance level of 99%. The table keeps 4 decimal places, the calculation keeps 8 decimal places.

Table A3. Layer soil moisture estimation model (30–50 cm).

Site	Intercept- a_0	LST- a_1	NDVI _{RES} - a_2	NDVI _{AG} - a_3	F-Value	R	RMSE
D1	-0.0014	0.0003	-0.0091	0.0181	4.6020 **	0.4652	0.0095
D2	-0.0332	0.0003	0.0570	0.0953	26.3842 **	0.7410	0.0140
D3	-0.0842	0.0005	0.0172	0.0802	147.0702 **	0.9336	0.0036
D4	-0.1455	0.0007	0.0316	0.0330	95.5330 **	0.9028	0.0058
D5	-0.4512	0.0020	-0.1234	0.0728	48.8376 **	0.8323	0.0213
D6	-0.2033	0.0010	-0.0737	0.0705	10.6289 **	0.6240	0.0277
D7	-0.3535	0.0014	0.1489	0.2710	100.0371 **	0.9066	0.0188
D8	-0.2611	0.0013	0.0147	0.1866	107.5899 **	0.9123	0.0132
D9	-0.3237	0.0013	0.1924	0.0761	6.2735 **	0.4826	0.0567
D10	-0.1469	0.0007	0.0054	0.3318	103.2531 **	0.9092	0.0108
D11	-0.0180	0.0002	0.1437	0.2159	22.7155 **	0.7154	0.0353
D12	-0.1346	0.0008	0.0908	0.0537	14.4754 **	0.7348	0.0149
D13	-0.3398	0.0016	-0.1759	0.1285	19.0697 **	0.7047	0.0547
D14	-0.7170	0.0030	-0.3272	0.0878	18.6426 **	0.7758	0.0381
D15	-1.7513	0.0071	-0.2116	0.0450	35.0906 **	0.7863	0.0667
D16	-0.3874	0.0017	-0.1079	0.0567	6.9133 **	0.4918	0.0526
D17	-0.4576	0.0019	0.1425	0.4975	39.1722 **	0.8530	0.0618
D18	-0.3296	0.0016	-0.0880	0.0489	12.7872 **	0.6092	0.0322
D19	-0.3036	0.0013	-0.0353	0.0737	34.1784 **	0.7823	0.0263
D20	-0.0590	0.0004	0.0769	0.1023	25.2061 **	0.7523	0.0131
D21	0.0503	-0.0002	0.0502	0.6640	20.0755 **	0.7230	0.0153
D22	-0.0449	0.0002	-0.0200	0.7046	31.0264 **	0.7673	0.0259
D23	-0.5755	0.0022	0.0430	0.1652	70.6508 **	0.8748	0.0202
D24	-0.2131	0.0008	0.0179	0.1207	70.9558 **	0.9157	0.0128
D25	-0.4455	0.0019	0.2208	0.1388	54.0855 **	0.8450	0.0211
D26	-0.4102	0.0019	0.4669	0.1138	30.2195 **	0.7632	0.0331
D27	-0.3371	0.0014	0.0287	0.0524	21.2821 **	0.7039	0.0233
D28	-0.0846	0.0007	0.1239	0.1617	60.3166 **	0.8757	0.0202
D29	-1.6336	0.0064	-0.2181	0.0271	34.8192 **	0.8145	0.0503
D30	-0.6545	0.0026	0.0989	0.0839	42.3720 **	0.8134	0.0249
D31	-0.5294	0.0022	0.0122	0.2322	46.7052 **	0.8285	0.0399

** represents F-test significance level of 99%. The table keeps 4 decimal places, the calculation keeps 8 decimal places.

Table A4. The 50–70 cm layer soil moisture estimation model.

Site	Intercept- a_0	LST- a_1	NDVI _{RES} - a_2	NDVI _{AG} - a_3	F-Value	R	RMSE
D1	0.0253	0.0001	−0.0361	0.1726	19.3090 **	0.6979	0.0123
D2	−0.1375	0.0007	0.0425	0.1023	38.1098 **	0.7985	0.0152
D3	−0.0882	0.0005	0.0236	0.0765	155.1495 **	0.9367	0.0036
D4	−0.1493	0.0007	0.0231	0.0354	120.8715 **	0.9209	0.0054
D5	−0.3495	0.0016	−0.1239	0.0601	33.9899 **	0.7815	0.0208
D6	−0.3934	0.0018	−0.0707	−0.0019	20.0979 **	0.7394	0.0219
D7	−0.1164	0.0006	0.0633	0.0714	112.0099 **	0.9154	0.0060
D8	−0.0750	0.0008	−0.0578	0.1556	126.9255 **	0.9242	0.0090
D9	−0.2302	0.0012	−0.1346	0.0672	20.0882 **	0.6964	0.0278
D10	−0.0524	0.0003	−0.2237	0.3529	90.7162 **	0.8998	0.0113
D11	0.0185	0.0002	0.1235	0.1380	19.0389 **	0.6839	0.0255
D12	−0.1324	0.0008	0.0654	0.0170	20.7468 **	0.7919	0.0089
D13	−0.3579	0.0017	−0.0768	0.1460	23.4037 **	0.7206	0.0563
D14	−0.4018	0.0017	−0.2710	0.0489	9.4123 **	0.6579	0.0295
D15	−0.5082	0.0024	−0.0496	0.2065	27.0967 **	0.7480	0.0667
D16	−0.0781	0.0007	−0.1116	0.1095	8.8637 **	0.5388	0.0458
D17	−0.2471	0.0010	0.1567	0.2524	24.4479 **	0.7906	0.0395
D18	−0.0561	0.0007	0.0170	0.0606	12.1061 **	0.5987	0.0263
D19	−0.2337	0.0011	−0.0544	0.0720	32.4551 **	0.7744	0.0250
D20	−0.1091	0.0005	0.0369	0.1078	22.2550 **	0.7315	0.0150
D21	0.0981	−0.0004	−0.1776	0.9557	12.3260 **	0.6341	0.0281
D22	0.0150	0.0001	−0.0915	0.5681	21.8802 **	0.7088	0.0245
D23	−0.5426	0.0021	0.0358	0.1850	51.7100 **	0.8395	0.0238
D24	−0.0146	0.0000	0.0540	0.0580	4.5765 **	0.5540	0.0159
D25	−0.2784	0.0012	0.0099	0.1675	40.9908 **	0.8088	0.0210
D26	−0.0808	0.0003	0.1109	0.0342	13.1810 **	0.6150	0.0117
D27	−0.1480	0.0007	0.0198	0.0610	26.5345 **	0.7420	0.0142
D28	−0.2307	0.0012	0.1268	0.1033	34.8308 **	0.7922	0.0229
D29	−0.4168	0.0020	−0.0756	0.0395	20.0238 **	0.7289	0.0274
D30	−0.6083	0.0025	0.0864	0.0694	48.0417 **	0.8302	0.0212
D31	−0.4414	0.0019	0.0115	0.1648	43.6817 **	0.8218	0.0308

** represents F-test significance level of 99%. The table keeps 4 decimal places, the calculation keeps 8 decimal places.

References

- Vereecken, H.; Huisman, J.A.; Franssen, H.H.; Bruggemann, N.; Bogaen, H.; Kollet, S.; Javaux, M.; Der Kruk, J.V.; Vanderborght, J. Soil hydrology: Recent methodological advances, challenges, and perspectives. *Water Resour. Res.* **2015**, *51*, 2616–2633. [[CrossRef](#)]
- Vereecken, H.; Huisman, J.A.; Bogaen, H.; Vanderborght, J.; Vrugt, J.A.; Hopmans, J.W. On the value of soil moisture measurements in vadose zone hydrology: A review. *Water Resour. Res.* **2008**, *44*, 44. [[CrossRef](#)]
- Tian, J.; Han, Z.B.; Bogaen, H.R.; Huisman, J.A.; Montzka, C.; Zhang, B.Q.; He, C.S. Estimation of subsurface soil moisture from surface soil moisture in cold mountainous areas. *Hydrol. Earth Syst. Sci. Discuss.* **2019**, in review. [[CrossRef](#)]
- Koster, R.D.; Dirmeyer, P.A.; Guo, Z.C.; Bonan, G.; Chan, E.; Cox, P.; Gordon, C.T.; Kanae, S.; Kowalczyk, E.; Lawrence, D.; et al. Regions of strong coupling between soil moisture and precipitation. *Science* **2004**, *305*, 1138–1140. [[CrossRef](#)] [[PubMed](#)]
- Seneviratne, S.I.; Corti, T.; Davin, E.L.; Hirschi, M.; Jaeger, E.B.; Lehner, I.; Orlowsky, B.; Teuling, A.J. Investigating soil moisture–Climate interactions in a changing climate: A review. *Earth-Sci. Rev.* **2010**, *99*, 125–161. [[CrossRef](#)]
- Oki, T.; Kanae, S. Global Hydrological Cycles and World Water Resources. *Science* **2006**, *313*, 1068–1072. [[CrossRef](#)]
- Federer, C.A. A Soil-Plant-Atmosphere Model for Transpiration and Availability of Soil Water. *Water Resour. Res.* **1979**, *15*, 555–562. [[CrossRef](#)]

8. Zhang, B.Q.; He, C.S.; Burnham, M.; Zhang, L.H. Evaluating the coupling effects of climate aridity and vegetation restoration on soil erosion over the Loess Plateau in China. *Sci. Total Environ.* **2016**, *539*, 436–449. [[CrossRef](#)]
9. Chen, R.; Kang, E.; Yang, J.; Zhang, J. A distributed daily runoff model of inland river mountainous basin. *Adv. Earth Sci.* **2003**, *18*, 198–206. [[CrossRef](#)]
10. Zhang, Y.M.; Chen, Y.N.; Pan, B.R. Distribution and floristics of desert plant communities in the lower reaches of Tarim River, southern Xinjiang, People's Republic of China. *J. Arid Environ.* **2005**, *63*, 772–784. [[CrossRef](#)]
11. Brocca, L.; Tullio, T.; Melone, F.; Moramarco, T.; Morbidelli, R. Catchment scale soil moisture spatial–temporal variability. *J. Hydrol.* **2012**, *422*, 63–75. [[CrossRef](#)]
12. Robock, A.; Vinnikov, K.Y.; Srinivasan, G.; Entin, J.K.; Hollinger, S.E.; Speranskaya, N.A.; Liu, S.X.; Namkhai, A. The Global Soil Moisture Data Bank. *B. Am. Meteorol. Soc.* **2000**, *81*, 1281–1299. [[CrossRef](#)]
13. Ochsner, T.E.; Cosh, M.H.; Cuenca, R.H.; Dorigo, W.A.; Draper, C.S.; Hagimoto, Y.; Kerr, Y.H.; Njoku, E.G.; Small, E.E.; Zreda, M. State of the Art in Large-Scale Soil Moisture Monitoring. *Soil Sci. Soc. Am. J.* **2013**, *77*, 1888. [[CrossRef](#)]
14. Njoku, E.G.; Jackson, T.J.; Lakshmi, V.; Chan, T.K.; Nghiem, S.V. Soil moisture retrieval from AMSR-E. *IEEE Trans. Geosci. Remote Sens.* **2003**, *41*, 215–229. [[CrossRef](#)]
15. Naeimi, V.; Scipal, K.; Bartalis, Z.; Hasenauer, S.; Wagner, W. An Improved Soil Moisture Retrieval Algorithm for ERS and METOP Scatterometer Observations. *IEEE Trans. Geosci. Remote Sens.* **2009**, *47*, 1999–2013. [[CrossRef](#)]
16. Wagner, W. Evaluation of the agreement between the first global remotely sensed soil moisture data with model and precipitation data. *J. Geophys. Res. Atmos.* **2003**, *108*, 4611. [[CrossRef](#)]
17. Wagner, W.; Hahn, S.; Kidd, R.; Melzer, T.; Bartalis, Z.; Hasenauer, S.; Figa-Saldana, J.; de Rosnay, P.; Jann, A.; Schneider, S.; et al. The ASCAT Soil Moisture Product: A Review of its Specifications, Validation Results, and Emerging Applications. *Meteorol. Z.* **2013**, *22*, 5–33. [[CrossRef](#)]
18. Kerr, Y.H.; Waldteufel, P.; Wigneron, J.-P.; Delwart, S.; Cabot, F.; Boutin, J.; Escorihuela, M.-J.; Font, J.; Reul, N.; Gruhier, C. The SMOS mission: New tool for monitoring key elements of the global water cycle. *Proc. IEEE* **2010**, *98*, 666–687. [[CrossRef](#)]
19. Entekhabi, D.; Njoku, E.G.; O'Neill, P.E.; Kellogg, K.H.; Crow, W.T.; Edelstein, W.N.; Entin, J.K.; Goodman, S.D.; Jackson, T.J.; Johnson, J. The soil moisture active passive (SMAP) mission. *Proc. IEEE* **2010**, *98*, 704–716. [[CrossRef](#)]
20. Rötzer, K.; Montzka, C.; Vereecken, H. Spatio-temporal variability of global soil moisture products. *J. Hydrol.* **2015**, *522*, 187–202. [[CrossRef](#)]
21. Xu, C.Y.; Qu, J.J.; Hao, X.J.; Cosh, M.; Prueger, J.; Zhu, Z.L.; Guttenberg, L. Downscaling of Surface Soil Moisture Retrieval by Combining MODIS/Landsat and In Situ Measurements. *Remote Sens.* **2018**, *10*, 210. [[CrossRef](#)]
22. Zhang, L.H.; He, C.S.; Zhang, M.M. Multi-Scale Evaluation of the SMAP Product Using Sparse In-Situ Network over a High Mountainous Watershed, Northwest China. *Remote Sens.* **2017**, *9*, 1111. [[CrossRef](#)]
23. Sandholt, I.; Rasmussen, K.; Andersen, J. A simple interpretation of the surface temperature/vegetation index space for assessment of surface moisture status. *Remote Sens. Environ.* **2002**, *79*, 213–224. [[CrossRef](#)]
24. Watson, K. Geologic applications of thermal infrared images. *Proc. IEEE* **1975**, *63*, 128–137. [[CrossRef](#)]
25. Price, J.C. On the analysis of thermal infrared imagery: The limited utility of apparent thermal inertia. *Remote Sens. Environ.* **1985**, *18*, 59–73. [[CrossRef](#)]
26. Li, J.K.; Islam, S. Estimation of root zone soil moisture and surface fluxes partitioning using near surface soil moisture measurements. *J. Hydrol.* **2002**, *259*, 1–14. [[CrossRef](#)]
27. Tobin, K.J.; Torres, R.; Crow, W.T.; Bennett, M.E. Multi-decadal analysis of root-zone soil moisture applying the exponential filter across CONUS. *Hydrol. Earth Syst. Sci. Discuss.* **2017**, *21*, 4403–4417. [[CrossRef](#)]
28. Lu, Z.; Chai, L.N.; Liu, S.M.; Cui, H.Z.; Zhang, Y.H.; Jiang, L.M.; Jin, R.; Xu, Z.W. Estimating time series soil moisture by applying recurrent nonlinear autoregressive neural networks to passive microwave data over the Heihe River Basin, China. *Remote Sens.* **2017**, *9*, 574. [[CrossRef](#)]
29. Mishra, V.; Ellenburg, W.L.; Markert, K.N.; Limaye, A.S. Performance evaluation of soil moisture profile estimation through entropy-based and exponential filter models. *Hydrol. Sci. J.* **2020**, *65*, 1036–1048. [[CrossRef](#)]

30. Babelt, A.; Viallefont-Robinet, F.; Jacquemoud, S.; Fabre, S.; Briottet, X. High-resolution mapping of in-depth soil moisture content through a laboratory experiment coupling a spectroradiometer and two hyperspectral cameras. *Remote Sens. Environ.* **2020**, *236*, 11. [[CrossRef](#)]
31. Parida, B.R.; Oinam, B.; Patel, N.R.; Sharma, N.; Kandwal, R. Land surface temperature variation in relation to vegetation type using MODIS satellite data in Gujarat state of India. *Int. J. Remote Sens.* **2008**, *29*, 4219–4235. [[CrossRef](#)]
32. Bai, M.; Mo, X.G.; Liu, S.X.; Hu, S. Contributions of climate change and vegetation greening to evapotranspiration trend in a typical hilly-gully basin on the Loess Plateau, China. *Sci. Total Environ.* **2019**, *657*, 325–339. [[CrossRef](#)] [[PubMed](#)]
33. Tucker, C.J. Red and photographic infrared linear combinations for monitoring vegetation. *Remote Sens. Environ.* **1979**, *8*, 127–150. [[CrossRef](#)]
34. Valor, E.; Caselles, V. Mapping land surface emissivity from NDVI: Application to European, African, and South American areas. *Remote Sens. Environ.* **1996**, *57*, 167–184. [[CrossRef](#)]
35. Dash, P.; Gottsche, F.M.; Olesen, F.S.; Fischer, H. Land surface temperature and emissivity estimation from passive sensor data: Theory and practice-current trends. *Int. J. Remote Sens.* **2002**, *23*, 2563–2594. [[CrossRef](#)]
36. Baldwin, D.; Manfreda, S.; Keller, K.; Smithwick, E.A.H. Predicting root zone soil moisture with soil properties and satellite near-surface moisture data across the conterminous United States. *J. Hydrol.* **2017**, *546*, 393–404. [[CrossRef](#)]
37. Yang, Y.T.; Guan, H.D.; Long, D.; Liu, B.; Qin, G.H.; Qin, J.; Batelaan, O. Estimation of Surface Soil Moisture from Thermal Infrared Remote Sensing Using an Improved Trapezoid Method. *Remote Sens.* **2015**, *7*, 8250–8270. [[CrossRef](#)]
38. Montzka, C.; Rötzer, K.; Bogena, H.; Sanchez, N.; Vereecken, H. A New Soil Moisture Downscaling Approach for SMAP, SMOS, and ASCAT by Predicting Sub-Grid Variability. *Remote Sens.* **2018**, *10*, 427. [[CrossRef](#)]
39. Tian, J.; Zhang, B.Q.; He, C.S.; Yang, L.X. Variability in Soil Hydraulic Conductivity and Soil Hydrological Response Under Different Land Covers in the Mountainous Area of the Heihe River Watershed, Northwest China. *Land Degrad. Dev.* **2017**, *28*, 1437–1449. [[CrossRef](#)]
40. Jin, X.; Zhang, L.H.; Gu, J.; Zhao, C.; Tian, J.; He, C.S. Modelling the impacts of spatial heterogeneity in soil hydraulic properties on hydrological process in the upper reach of the Heihe River in the Qilian Mountains, Northwest China. *Hydrol. Process.* **2015**, *29*, 3318–3327. [[CrossRef](#)]
41. Ye, Z.; Hong, T.; Chileshe, J.M.; Wen, T.; Feng, R.J. Multi-factor evaluation and modeling correction of EC-5 and 5TE soil moisture content sensors. *Trans. Chin. Soc. Agric. Eng.* **2012**, *28*, 157–166. [[CrossRef](#)]
42. Tian, J.; Zhang, B.Q.; He, C.S.; Han, Z.B.; Bogena, H.R.; Huisman, J.A. Dynamic response patterns of profile soil moisture wetting events under different land covers in the Mountainous area of the Heihe River Watershed, Northwest China. *Agric. For. Meteorol.* **2019**, *271*, 225–239. [[CrossRef](#)]
43. Didan, K. *MOD13A2 MODIS/Terra Vegetation Indices 16-Day L3 Global 1km SIN Grid V006*; LP DAAC: Sioux Falls, SD, USA, 2015. [[CrossRef](#)]
44. Wan, Z.; Hook, S.; Hulley, G. *MOD11A2 MODIS/Terra Land Surface Temperature/Emissivity 8-Day L3 Global 1km SIN Grid V006*; LP DAAC: Sioux Falls, SD, USA, 2015. [[CrossRef](#)]
45. Marcal, A.R.S.; Wright, G.G. The use of ‘overlapping’ NOAA-AVHRR NDVI maximum value composites for Scotland and initial comparisons with the land cover census on a Scottish regional and District basis. *Int. J. Remote Sens.* **1997**, *18*, 491–503. [[CrossRef](#)]
46. Cihlar, J.; Ly, H.; Li, Z.; Chen, J.M.; Pokrant, H.; Huang, F. Multitemporal, multichannel AVHRR data sets for land biosphere studies—Artifacts and corrections. *Remote Sens. Environ.* **1997**, *60*, 35–57. [[CrossRef](#)]
47. Kobayashi, H.; Dye, D.G. Atmospheric conditions for monitoring the long-term vegetation dynamics in the Amazon using normalized difference vegetation index. *Remote Sens. Environ.* **2005**, *97*, 519–525. [[CrossRef](#)]

48. Jonsson, P.; Eklundh, L. Seasonality extraction by function fitting to time-series of satellite sensor data. *IEEE Trans. Geosci. Remote Sens.* **2002**, *40*, 1824–1832. [[CrossRef](#)]
49. Beck, P.S.A.; Atzberger, C.; Hogda, K.A.; Johansen, B.; Skidmore, A.K. Improved monitoring of vegetation dynamics at very high latitudes: A new method using MODIS NDVI. *Remote Sens. Environ.* **2006**, *100*, 321–334. [[CrossRef](#)]



© 2020 by the authors. Licensee MDPI, Basel, Switzerland. This article is an open access article distributed under the terms and conditions of the Creative Commons Attribution (CC BY) license (<http://creativecommons.org/licenses/by/4.0/>).